Chen HY, Bucher N, Hartung S, Li L, Friedl J, Liou HP, Sun CL, Stimming U, Srinivasan M.

A Multi-Walled Carbon Nanotube Core with Graphene Oxide Nanoribbon Shell as Anode Material for Sodium Ion Batteries.

***Advanced Materials Interfaces* 2016, 3(20).**

WILEY-VCH

DOI: 10.1002/((please add manuscript number))
Article type: Full paper

A multi-walled carbon nanotube core with graphene oxide nanoribbon shell as anode material for sodium ion batteries

Han-Yi Chen, [1,2,3,4] *Nicolas Bucher,* [1,2,3] *Steffen Hartung,* [1,2,3] *Linlin Li,* [1,3] *Jochen Friedl,* [1,5] *Huei- Ping Liou,*[6] *Chia-Liang Sun,*[6,7] *Ulrich Stimming,*[1, 2,5*] *and Madhavi Srinivasan,* [1, 3, 8*]

[1] TUM CREATE, 1 CREATE Way, #10-02 CREATE Tower, 138602 Singapore
[2] Department of Chemistry, Technische Universität München, Lichtenbergstraße 4, 85748 Garching, Germany
[3] School of Materials Science and Engineering, Nanyang Technological University, 639798 Singapore
[4] Department of Materials Science and Engineering, National Tsing Hua University, 101, Sec. 2, Kuang-Fu Road, Hsinchu 30013,Taiwan
[5] School of Chemistry, Bedson Building, Newcastle University, Newcastle upon Tyne NE1 7RU, United Kingdom
[6] Department of Chemical and Materials Engineering, Chang Gung University, Kwei-Shan, Taoyuan 333, Taiwan
[7] Department of Neurosurgery, Chang Gung Memorial Hospital, No. 5, Fu-Shing Rd., Guishan, Taoyuan 333, Taiwan
[8] Energy Research Institute @ NTU (ERI@N), Research Techno Plaza, 50 Nanyang Drive, 637553 Singapore

[*] Prof. Madhavi Srinivasan
School of Material Science and Engineering,
Nanyang Technological University, 639798 Singapore
E-mail: madhavi@ntu.edu.sg

[*] Prof. Ulrich Stimming
School of Chemistry, Bedson Building, Newcastle University, Newcastle upon Tyne NE1 7RU, United Kingdom
E-mail: Ulrich.Stimming@newcastle.ac.uk

Keywords: Na-ion batteries, multi-wall carbon nanotubes, graphene oxide nanoribbons, functionalization, Na-ion anode

Abstract

A novel core–shell heterostructure with multi-walled carbon nanotubes (MWCNTs) as the core and graphene oxide nanoribbons (GONRs) as the shell (MWCNT@GONR) is investigated for the first time as anode material for Na-ion batteries (NIBs) in this study. The MWCNT@GONR material with carboxylic acid groups has been synthesized through unzipping of MWCNTs by a microwave-assisted process. The influence of the amount of carboxylic acid groups on the electrochemistry of MWCNT@GONR is investigated in this work by applying thermal treatment at different temperatures. In this MWCNT@GONR core-shell structure, the MWCNTs between flat GONR sheets prevent the restacking problem of graphene and enable penetration of the electrolyte. MWCNTs provide high electronic conductivity and direct electron transfer path while GONRs provide high surface area and defect sites (carboxylic acid groups, COOH-) that can adsorb more Na ions on the surface thereby increasing capacity. MWCNT@GONR provides high capacity (317 mA h g^{-1}) at a current density of 50 mA h g^{-1} in the 2nd cycle. The capacity of MWCNT@GONR decreases when the amount of COOH- groups decreases, indicating that COOH- groups can help to adsorb Na ions. A full cell using MWCNT@GONR as anode and P2-Na_xMnO_2 as cathode is fabricated and it exhibits a high energy density of 99 Wh kg^{-1} which successfully demonstrates that MWCNT@GONR is a promising anode material for NIB applications.

1. Introduction

Currently, lithium-ion batteries (LIBs) are the leading energy storage technology due to their high energy density.[1] However, the challenges of LIBs for large-scale energy storage applications are the scarcity of lithium (only 20 ppm in the earth's crust) and its high cost.[2-5] Na-ion batteries (NIBs) have attracted significant attention because of the high abundance of sodium (~ 2.5 % in the earth's crust) and potential cost advantages

over LIBs. Therefore, NIBs are a promising candidate for large-scale energy storage.[4, 5] As alkali metal, Na has chemical properties similar to Li, which is assumed to simplify transfer of materials and techniques from LIB to NIB technology. However, the higher standard reduction potential ($E^0_{Na^+/Na}$ = −2.17 V vs. standard hydrogen electrode (SHE); $E^0_{Li^+/Li}$ = −3.04 V vs. SHE)[3] and the fact that Na is heavier than Li result in a lower energy density for NIBs. Nevertheless, the cost advantage over LIBs renders NIBs a promising candidate for large-scale applications.[3, 4]

Graphite is the most commonly used anode material for LIBs, but it does not allow Na ions to intercalate reversibly due to unfavorable thermodynamical processes.[6, 7] Varies anode materials have been studied for NIBs, such as carbonaceous materials,[2-4, 8, 9] metal oxides/sulfides,[10-23] sodium alloys, [24-33] phosphorus,[24-26] phosphides,[27] organic compounds,[37,38] and polyoxometalates.[6] Conversion type metal oxides/sulphides exhibit high capacities such as $NiCoO_4$,[14] Fe_3O_4,[15] MoO_3,[16] CuO,[17] Ni_3S_2,[18] MoS_2,[19] SnS_2,[20] SnS,[20] Co_9S_8,[21] FeS,[22] and Sb_2S_3.[23] exhibit high capacities. However, large potential hysteresis (for some larger than 1 V), low initial coulombic efficiency (30–70%) and poor cycling stability restrict the practical application of conversion type metal oxides/sulfides in NIBs.[7] Several metals such as tin and antimony provide high capacities in NIBs by forming sodium alloys.[7, 28-37] Large initial discharge capacities of 878 mA h g^{-1} for Sn and ~ 600 mA h g^{-1} for Sb could be obtained. Nevertheless, large volume expansion (420 % volume change for Sn and 290 % for Sb) during the formation of alloys results in fast capacity fading.[7, 28, 29]

Carbon-based materials are the most promising candidates among above materials because they are low-costinexpensive, easily obtainable, and environmentally friendly. They can also be used as buffer matrixes for conversion and alloy type anode for

preventing the volume expansion during the Na ion (de-)insertion.[30-37] Potential carbon materials which have been explored are hard carbon,[8] expanded graphite,[2] reduced graphene oxide (rGO),[3] and nitrogen-doped carbon fibers.[9] Hard carbon exhibits high cycling stability at C/10 for over 100 cycles with ~~the~~ a capacity of more than 300 mAh g^{-1} as reported by Palacin et al.[8] However, the capacity at 20 C is only around 150 mAh g^{-1} due to its lower electronic conductivity ~~as~~ compared to other carbon materials such as graphite and rGO. Expanded graphite which has been reported by Wen et al. provides excellent cycling stability with a very low capacity decay rate of ~ 0.013% per cycle from the 11th cycle to the 2,000th cycle when cycled at 100 mA g^{-1}.[2] Nevertheless, expanded graphite shows a poor rate capability as indicated by a drop from 284 mAh g^{-1} at 20 mA g^{-1} to 91 mAh g^{-1} at 200 mA g^{-1}. Recently, rGO has received much attention due to ~~its excellent~~ properties such as high electronic conductivity, good chemical stability, and high surface area.[38, 39] Wang et al. reported a rGO anode which exhibits reversible capacities of 217.2 mAh g^{-1} at 40 mA g^{-1} and 95.6 mAh g^{-1} at a high current rate of 1000 mA g^{-1}~~, showing good rate capability~~.[3] Nonetheless, the capacity in the 1st cycle is highly irreversible, and the rGO sheets restack during cycling which results in poor capacity retention.[38] Functionalized N-doped carbon nanofibers (FN-CNFs) have been reported with a capacity of 134.2 mA h g^{-1} after 200 cycles at a current density of 200 mA g^{-1} (capacity retention of 88.7%).[9] The interconnected porous carbon nanofibers ease Na ion transport and provide a continuous path for electron transport. The O- and N-containing functional groups on the surface of FN-CNFs not only accelerate the surface redox reactions but also induce a large number of defects on the graphene layer which enhances sodium ion absorption properties resulting in high rate performance.[9] So far, there is no carbon anode material which can provide high capacity, good rate

capability, good capacity retention, and high coulombic efficiency in the 1st cycle ~~in~~ at the same time.

In our work, we report a novel core–shell structure with multi-walled carbon nanotubes (MWCNTs) as the core and graphene oxide nanoribbons (GONRs) as the shell (MWCNT@GONR). It is synthesized by unzipping of MWCNTs in a microwave-assisted process. The MWCNTs ~~surrounded by flat graphene sheets~~ are intended to prevent the restacking ~~problem~~ of the flat graphene sheets, thereby ~~enabling the penetration of the electrolyte. This also helps to increase~~ increasing the coulombic efficiency in the 1st cycle ~~and the capacity retention.~~. MWCNTs provide high electronic conductivity and a direct electron transfer path which ~~can increase~~enahnces the rate capability, while GONRs provide high surface area and defect sites (carboxylic acid groups, –COOH) that can adsorb more Na^+ on the surface ~~so as~~ to increase the capacity. In order to investigate the influence of carboxylic acid groups on Na^+ adsorption, the MWCNT@GONR sample was treated at different temperatures (300 °C, 600 °C, and 900 °C for 1 hr in Argon atmosphere) to remove functional groups. A comparison with commercial graphene nanopowder (GNP) and MWCNTs employed as anode materials is conducted.

2. Results and discussion

2.1. Material characterization

Brunauer-Emmett-Teller (BET) measurements of the surface area are obtained for MWCNTs and MWCNT@GONR by N_2 adsorption-desorption isotherms. These isotherms are shown in **Figure 1a**. The surface area of the MWCNTs and sample MWCNT@GONR are 29.3 and 38.2 $m^2 g^{-1}$, respectively. This indicates that the core–shell MWCNT@GONR which is fabricated from the facile unzipping of MWCNTs by microwave-assisted synthesis exhibits a higher surface area than MWCNT resulting in

the possibility to attract more Na ion on the surface of MWCNT@GONR. The Barrett-Joyner-Halenda (BJH) pore size distribution of MWCNT and MWCNT@GONR is shown in **Figure 1b.** The pore diameters show a size distribution ranging from ~ 3 nm to ~ 120 nm, and most of these pores exhibit a narrower distribution of mesopores centered between 3 and 7 nm.

Figure 2 displays bright-field transmission electron microscopy (TEM) images of GNP (a), MWCNT (b), MWCNT@GONR (c) , MWCNT@GONR annealed at 300 °C for 1 hr (MWCNT@GONR-300°C) (d) , MWCNT@GONR annealed at 600 °C for 1 hr (MWCNT@GONR-600°C) (e), and MWCNT@GONR annealed at 900 °C for 1 hr (MWCNT@GONR-900°C) (f). On the TEM images a smooth and planar surface is observed for GNP, while the MWCNTs shows a tube-like structure. For the MWCNT@GONR samples, graphene oxide sheets are wrapped around nanotube cores. During thermal treatment at 300 °C, 600°C, and 900°C, the MWCNT@GONRs maintain their morphology. **Figure 3** shows scanning electron microscopy (SEM) images of GNP (a), MWCNT (b), MWCNT@GONR (c), MWCNT@GONR-300°C (d), MWCNT@GONR-600°C (e), and MWCNT@GONR-900°C (f). On the SEM images it can be observed that the GNP sheets stack together, while the tube-liked MWCNTs intertwine with each other. The MWCNT@GONRs (with and without heat treatment) have MWCNT as core and planar graphene sheets surrounding the outside.

Figure 4a shows FTIR spectra of the pristine MWCNT, MWCNT@GONR, MWCNT@GONR-300°C, MWCNT@GONR-600°C, and MWCNT@GONR-900°C samples. The stretching C=O and –OH vibration of the carboxylic groups (–COOH) at 1722 cm^{-1} and 3417 cm^{-1} are observed for MWCNT@GONR, while those peaks are missing in the pristine MWCNT.[40] This indicates that during the unzipping process of MWCNT, carboxylic groups on the surface of MWCNT@GONR are created. The peaks of carboxylic groups can also be observed for MWCNT@GONR-300°C and

MWCNT@GONR-600°C. The absence of these bands in the spectrum of MWCNT@GONR-900°C indicates successful removal of -COOH group by the annealing step under argon. The aromatic C=C stretch is observed at around 1582 cm^{-1} in the spectra of MWCNT@GONRs and 1635 cm^{-1} in the spectra of MWCNT.[40-42] This shift might due to the changes in the MWCNT structure after unzipping processes.[43]

Figure 4b displays evolution of sample weight over temperature for MWCNT, MWCNT@GONR, MWCNT@GONR-300°C, MWCNT@GONR-600°C, and MWCNT@GONR-900°C recorded by thermogravimetric analysis (TGA) under argon. Almost no weight loss can be observed for the pristine MWCNT sample, indicating that no functional groups are present on the surface. The MWCNT@GONR sample exhibits a significant weight loss (~ 31 wt %) from ~200 to ~900 °C which indicates desorption of functional groups. Desorption temperature and the CO and CO_2 signal detected by a mass spectrometer (MS) (**Figure 4c**) imply that mostly –COOH are present on the surface. Many peaks can be observed in the MS spectra indicating a broad distribution of functional groups was generated, and they will be analyzed by X-ray photoelectron spectrometer (XPS) later. The weight loss of MWCNT@GONR-300°C, MWCNT@GONR-600°C, and MWCNT@GONR-900°C is 26 wt %, 11 wt %, and 2 wt %, respectively. This indicates that less functional groups are present on the surface of MWCNT@GONR when the annealing temperature during the thermal treatment is increased. These TGA results are consistent with FTIR. The TGA curve of MWCNT@GONR-900°C with only 2 wt % weight loss implies that the surface functional groups have almost been removed by the previous applied thermal treatment.

The surface composition was analysed by XPS and the corresponding C1s peak spectra with peak binding energies and corresponding atomic percentages of GNP,

MWCNT, MWCNT@GONR, MWCNT@GONR-300°C, MWCNT@GONR-600°C, and MWCNT@GONR-900°C are shown in **Figure 5**.[44] C=C, C–C and C–O functional groups are found in all of the carbon materials. The numbers after the bonds indicate the atomic ratio as compared to the main C–C peak. MWCNT@GONR shows a high amount of C–O and extra C=O and O–C=O functional groups. The amount of O-containing functional groups was significantly decreased after thermal treatment.

FTIR is qualitative analysis which provides the characteristic of the functional groups; while XPS is qualitative and semi-quantitative analysis which provides the characteristic and the corresponding atomic percentages of the functional groups on the surface. TGA-MS is quantitative analysis that provides the amount of functional groups on whole MWCNT@GONR. FTIR, TGA–MS, and XPS analyses demonstrate that the unzipping process generates significant amount of O-containing functional groups on MWCNT@GONR while the thermal treatment lowers the amount of O-containing functional groups.

X-ray diffraction (XRD) patterns of MWCNT, MWCNT@GONR, MWCNT@GONR-300°C, MWCNT@GONR-600°C, and MWCNT@GONR-900°C are shown in **Figure 6a**. The pattern of the pristine MWCNT shows an intense peak at $2\theta = 26.2°$ corresponding to the (002) reflection, while other diffraction peaks at 2θ of 42.7°, 54.3° and 77.6° are indexed to the (100), (004) and (110) reflections.[40] The pattern of MWCNT@GONR exhibits a MWCNT characteristic reflection at 26.2° 2θ (d-spacing ~3.4 Å) and a broad shoulder at 23.7° 2θ (d-spacing ~ 3.8 Å), indicating large distribution of GONR interlayer spaces with O-containing functional groups outside of the MWCNT core. After thermal treatment, the interlayer spacing of MWCNT@GONR successively approaches the interlayer spacing of that of MWCNT owing to the removal of O-containing functional groups.[45]

Raman Spectroscopy was employed to quantify the graphitic character of the carbon materials. **Figure 6b** shows the Raman spectra of MWCNT, MWCNT@GONR, MWCNT@GONR-300°C, MWCNT@GONR-600°C, and MWCNT@GONR-900°C with the ratio of the D-band and G-band intensity (I_D/I_G) where the peak heights are determined by Lorentz curve-fitting. A higher I_D/I_G ratio indicates more defect sites on the carbon materials. The I_D/I_G ratio is only 0.1 for pristine MWCNTs, indicating graphitic character with few defects. After the unzipping process, the I_D/I_G ratio of MWCNT@GONR jumps to 0.79 reflecting highly amount of defects due to the deterioration of the graphitic structure.[46] Thermal treatment heals lattice defects on MWCNT-GONR, thus the I_D/I_G ratio of MWCNT@GONR-300°C and MWCNT@GONR-600°C slightly decreased.[46] MWCNT@GONR-900°C has a higher I_D/I_G ratio than MWCNT@GONR-300°C and MWCNT@GONR-600°C indicating higher amounts of disordered carbon.[47] This can be explained by the removal of the epoxide group, which causes in-plane C=C cracking.[47]

2.2. Electrochemical performance

To understand the electrochemical properties of GNP, MWCNT, MWCNT@GONR, MWCNT@GONR-300°C, MWCNT@GONR-600°C, and MWCNT@GONR-900°C, these materials were used as electrode in half-cell experiments. The half-cells are first discharged, and subsequently cycled between 0.005 V and 3 V vs. Na^+/Na. Cyclic voltammetry (CV) curves for all samples are shown in **Figure 7**. The CV curves were recorded at a scan rate of 0.1 mV s^{-1} and the first three cycles are shown. Two main reduction peaks ~~at~~ in the first cycle can be observed in the CV curves. The contribution of the irreversible formation of solid-electrolyte interphase (SEI) layer can be observed at ~ 0.45 V.[48] ~~However, t~~The carboxylic groups on the surface of MWCNT@GONR and MWCNT@GONR-300C might react with electrolyte irreversibly and continuously

which show a broad peak.[49] Therefore, the peaks at ~0.45 V in MWCNT@GONR and MWCNT@GONR-300C are not as obvious as MWCNT@GONR-900C (with only 2 wt% carboxylic groups). The reduction peak at ~ 0.005 V could be the adsorption of Na^+ onto the graphene sheets and/or active sites.[3, 50] In the oxidation curves, the peaks at ~ 0.085 V for GNP, MWCNT@GONR, and MWCNT@GONR-300°C, and at ~ 0.010 V for MWCNT, MWCNT@GONR-600°C, and MWCNT@GONR-900°C, could be the desorption of Na^+ from the graphene layers.[50] The CV curve of GNP ~~presents~~ shows a highly irreversible current in the initial cycle due to the SEI layer formed on the high surface area (**Figure 7a**). The current in the following cycles ~~is~~ continually decreases which can be explained by restacking of the graphene sheets.[7] MWCNT@GONR exhibits a much higher ~~specific~~ normalised current and less irreversible current than GNP demonstrating that by adding carbon nanotubes between graphene sheets the restacking effect in graphene can be diminished and the penetration of the electrolyte can be improved.[44] The higher specific current of MWCNT@GONR as compared to MWCNT can be attributed to the enlarged surface area and more functional groups after the unzipping process. To investigate the effect of O-containing functional groups on the electrochemical performance of MWCNT@GONR, the CV curves of MWCNT@GONR with thermal treatment at different temperatures (300, 600, and 900 °C) are shown in **Figure 7(~~e~~d)-(f)**. The higher the annealing temperature the fewer O-containing functional groups decorate the sample as evidenced by FTIR, TGA-MS, and XPS. In the potential range of 0.75 ~ 3 V, the specific currents decrease when the annealing temperature is increased, indicating a strong evidence that the redox reaction between sodium and functional groups on the surface of MWCNT@GONR provide more sites for sodium storage.[9]

Here, we propose the mechanisms of enhanced Na^+ storage capability of MWCNT@GONR, as shown in **Scheme 1**. After the unzipping process, the increased

Field Code Changed

Field Code Changed

surface area provides more sites to attract Na^+, while the defects and functional groups at the surface of MWCNT@GONR are highly active and therefore can absorb Na^+. Besides, the defects enable Na^+ to insert through the vacancies into the interlayers which results in more sites for the accommodation of Na^+.

Figure 8 displays galvanostatic charge discharge (GCD) profiles of GNP, MWCNT, MWCNT@GONR, MWCNT@GONR-300°C, MWCNT@GONR-600°C, and MWCNT@GONR-900°C at a current density of 50 mA g^{-1} in the first three cycles. In **Figure 8c**, MWCNT@GONR shows a steady insertion of Na^+ in the potential range between 0.005 ~ 2.6 V vs. Na^+/Na which is not observed in GNP (**Figure 8a**) and MWCNT (**Figure 8b)**. These nearly linear charge/discharge curves imply some capacitive behaviour with continuous insertion of Na-ions.[6, 9] ~~It~~ This results in a high capacity which is mainly contributed from the core-shell structure that has higher surface area than MWCNT while preventing restacking of graphene sheets as well as the surface defects and functional groups.[9, 44] It's worth noting that the low initial columbic efficiency of ~11 % ~~is~~ observed in GNP ~~which can be probably~~was ~~be~~ attributed to the irreversible formation of a SEI layer due to the decomposition of electrolyte on materials with large surface areas and the restacking problem of graphene sheets in the literature.[3, 7] The initial columbic efficiency of MWCNT@GONR is ~70 % which is much higher than GNP, indicating the ~~elimination~~ mitigation of the restacking problem ~~in graphene with the core-shell structure~~.[44] However, coulombic efficiency is still not very high - carboxylic acid groups on the surface might, at least partially, react with the electrolyte which could also attribute to the irreversible processes in the first cycle.[49] The SEI layer on the MWCNT@GONR can be detected by XPS as shown in **Figure S1**. The surface layer of MWCNT@GONR after cycling is composed of a chemisorbed oxygen, Na_2CO_3, $NaCO_3R$ (R = different long-chain alkyl groups), NaOR, Na_2O, and NaCl. These are

most likely formed ~~–~~by decomposition of the electrolyte.[51, 52] When increasing the annealing temperature, the capacity in the potential range between 0.75 ~ 2.6 V decreases due to the decrease of defects and functional groups.[53] ~~However, this results in a higher average potential for MWCNT@GONR (at ~ 0.78 V vs. Na/Na^+) than MWCNT@GONR-900°C (at ~ 0.38 V vs. Na/Na^+).~~

The cycling performance of GNP, MWCNT, MWCNT@GONR, MWCNT@GONR-300°C, MWCNT@GONR-600°C, and MWCNT@GONR-900°C at a current density of 50 mA h g^{-1} is shown in **Figure 9a**. MWCNT@GONR has the largest reversible discharge capacity after the second cycle. The capacities decrease with the decreasing amount of O-containing functional groups. It is worth noting that MWCNT@GONR samples, with or without thermal treatment, show much a higher capacity than MWCNT and GNP. MWCNT@GONR exhibits a ~~high~~ capacity up to 317 mA h g^{-1} in the 2^{nd} cycle and ~ 200 mA h g^{-1} after 100 cycles with a coulombic efficiency of ~100 %. The higher capacity of MWCNT@GONR as compared to GNP implies that it might be a potential carbon buffering matrix to replace graphene which can form carbon composites with alloy type or metal oxide/sulphide anode materials in order to enhance the electrical connectivity, increase the surface area, and prevent volume expansion. The lower capacity retention of MWCNT@GONR as compared to MWCNT@GONR-900°C might be due to the large amount of O-containing functional groups on MWCNT@GONR that results in some irreversible sodium adsorption onto the defect sites.[9]

The capacity at different current densities is shown in **Figure 9b**. At higher current densities the discharge capacities decrease. The capacities at a current density of 20 mA h g^{-1} (6^{th} cycle) for MWCNT, MWCNT@GONR, MWCNT@GONR-300°C, MWCNT@GONR-600°C, and MWCNT@GONR-900°C are 64, 361, 320, 234, and 153 mA h g^{-1}, respectively. MWCNT@GONR shows higher capacity even at higher

current rates than others which is attributed to the higher amount of surface defects and functional groups.[9] Even at high current density of 2000 mA g^{-1}, MWCNT@GONR exhibits a capacity of 165 mA h g^{-1} indicating a high rate capability. When changing the current rate again back to 20 mA g^{-1} (from 37th cycle to 50th cycle), the capacities are rather stable.

To demonstrate the potential application of MWCNT@GONR as anode in a Na metal-free battery, a proof of concept test by combining a MWCNT@GONR anode and a P2-Na_xMnO_2 cathode was carried out.[54] **Figure 10a** shows the GCD profiles of the P2-Na_xMnO_2 cathode with a reversible capacity of 192 mAh g^{-1} at a current density of 20 mA g^{-1}. **Figure 10b** shows the GCD profiles of MWCNT@GONR half-cell in the 5th discharge cycle and P2-Na_xMnO_2 half-cell in the 2nd charge cycle. To eliminate the influence of SEI formation, the MWCNT@GONR half-cell was charged and discharged for 5 cycles, while the P2-Na_xMnO_2 half-cell was charged and discharged for 2 cycles before fabricating the full cell. The mass ratio was selected according to the equation $q_a = q_c$ $(C_a m_a = C_c m_c)$, where C is specific capacity, m is mass, and the indices a and c represent anode and cathode.[55] The specific capacities of MWCNT@GONR and P2-Na_xMnO_2 are calculated at a current density of 20 mA g^{-1} from the GCD curves in **Figure 10b**. They were 344 mA h g^{-1} for MWCNT@GONR obtained in the potential range of 0.005 ~ 2.2 V vs. Na/Na^+ and 164 mA h g^{-1} for P2-Na_xMnO_2 obtained in the potential range of 2.2 ~ 3.8 V vs. Na/Na^+, respectively. According to this, a mass ratio of MWCNT@GONR: P2-Na_xMnO_2 = 1 : 2.1 is shown in this work.

The electrochemical performance of the MWCNT@GONR// P2-Na_xMnO_2 full cell in the voltage window of 0 V to 4 V is shown in **Figure 10c** and **10d.** Initial charge capacity of the full cell is close to 466 mA h g^{-1} based on the mass of MWCNT@GONR after charging to 4 V. The discharge capacities are 183 mA h g^{-1}

based on the mass of MWCNT@GONR and 90 mA h g^{-1} based on the mass of P2-Na_xMnO_2 at the 1st cycle with an average potential of 1.65 V. The irreversible capacity in the 1st cycle might be due to side reactions from both electrodes. The following cycles are rather stable with a small amount of degradation. At the 20th cycle, the capacity is 140 mA h g^{-1} based on the mass of MWCNT@GONR (capacity retention ~ 77 %) with a coulomb efficiency of 88 %. The low coulomb efficiency is probably due to electrolyte decomposition of $NaClO_4$ in EC/DC above 3.8V.[56] The energy density of the MWCNT@GONR// P2-Na_xMnO_2 full cell is 99 Wh kg^{-1} based on the total mass of the cathode and anode active materials. This value is higher than for other ~~system~~ cell chemistries reported in literature, such as rGO/Sb_2S_3—$Na_{2/3}Ni_{1/3}Mn_{2/3}O_2$ NIB system with an energy density of 80 Wh kg^{-1} where the cathode is similar ~~with~~ to P2-Na_xMnO_2.[57] These results demonstrate that MWCNT@GONR is a potential anode material for Na-ion battery. Although the energy density of our NIB system is lower than a $LiFePO_4$–$Li_4Ti_5O_{12}$ LIB system which has an energy density of 142 Wh kg^{-1}, [57] it can be improved by further optimization, e.g. by optimizing the mass ratio or using other cathode materials with higher capacity.

3. Conclusion

In summary, a core–shell structure of MWCNT@GONR with carboxylic acid groups has been successfully synthesized by unzipping of MWCNTs with the help of microwave energy. It has been demonstrated to be a promising anode material for NIBs. The core-shell structure of MWCNT@GONR prevents the restacking problem of graphene by adding MWCNTs between GONR sheets thus enabling the electrolyte to penetrate between the GONR sheets.[44] MWCNTs provide a direct electron transfer path with high electronic conductivity while GONRs provide high surface area with carboxylic acid groups which facilitate the adsorption of Na ions on the surface and

increase capacity.[9] To investigate the influence of the carboxylic acid groups, the amount of those functional groups has been reduced successfully by applying thermal treatment at 300 ~ 900 °C, as confirmed by FTIR, TGA, and XPS. MWCNT@GONR with carboxylic acid groups provides higher capacities (317 mA h g^{-1}) than commercial MWCNT (54 mA h g^{-1}) and GNP (100 mA h g^{-1}) at a current density of 50 mA h g^{-1} in the 2nd cycle. This implies that MWCNT@GONR might be a potential carbon buffering matrix to replace graphene in forming the carbon composites with alloy type or metal oxide/sulphide anode materials. Capacities decrease when the amount of COOH- groups on MWCNT@GONR is reduced after thermal treatment, indicating that surface defects and functional groups on MWCNT@GONR provide more sites for sodium storage. The easily-synthesized and cost-efficient MWCNT@GONR (~ 5 USD/g for production on lab scale without the cost of electricity and manpower, as compared to commercial rGO ~ 200 USD/g from Carbon solution Ltd.) shows high capacities at various cycling rates with good stability, and it is a safe and environmentally friendly candidate for commercial energy storage applications. To demonstrate a practical device application of MWCNT@GONR, a full cell with MWCNT@GONR as anode and P2-Na_xMnO_2 as cathode was assembled and exhibited a high energy density of 99 Wh kg^{-1}. This successful proof-of-concept test confirmed the potential of MWCNT@GONR as a promising anode candidate for NIBs.

4. Experimental Section

Materials

MWCNTs were used as received from Mitsui & Co. (diameter = 40~90 nm; length = >10 μm). GNP (UR-graphene 12, 99.2%, special surface area ~ 80 m^2 g^{-1}, average flake thickness ~ 12 nm, with 30 to 50 monolayers, average particle (lateral) size ~ 4.5 mm) was obtained from Uni-Region. Sulfuric acid (H_2SO_4, 98 %), phosphoric acid

(H_3PO_4, 85 %), and potassium permanganate ($KMnO_4$) were obtained from J. T. Baker.

Microwave-assisted synthesis of MWCNT@GONR

The MWCNT@GONR was synthesized using the method described in our previous publications.[44, 58] 0.05 g MWCNTs were suspended in a H_2SO_4/H_3PO_4 solution (molar ratio 9:1) followed by a microwave treatment (microwave reactor, CEM-Discover) at 200 W for 2 min. 0.25 g $KMnO_4$ was added to the solution, and then treated with the same micro-wave power at 65 °C for 8 min. In this synthesis procedure, a weak acid, H_3PO_4, was employed to meliorate the selectivity of the oxidative unzipping process, assuming the in situ protection of the vicinal diols formed on the basal plane of graphene during oxidation and therefore prevents their over oxidation and subsequent hole generation.

The MWCNT@GONR solution was filtered by a Millipore membrane with a pore size of 0.1 μm. The final product was washed with deionized (DI) water several times and dried at 80 °C overnight. The as-prepared MWCNT@GONR contained oxygen-containing functional groups (carboxylic acid groups). A thermal treatment in a tube furnace at temperature range from 300 °C to 900 °C was applied with an argon flow of 5 cm^3 min^{-1} for MWCNT@GONR reduction.

Characterization of MWCNT@GONR

The Brunauer Emmetand Teller (BET) surface area of MWCNT@GONR and MWCNT were determined by N_2 adsorption-desorption isotherms at 77 K. The morphology was characterized by field emission scanning electron microscope (FESEM, JEOL JSM 7600F) and high resolution transmission electron microscopy (HRTEM, JOEL-JSM 2010F). A thermogravimetric analysis coupled with mass

spectroscopy (TGA-MS) setup (STARe TGA from Mettler Toledo connected with Thermostar GSD3200 from Pfeiffer Vacuum) was used to determine the decomposition temperature of the surface functional groups. The samples were heated from 25 °C to 1000 °C applying a constant temperature ramp of 10 °C /min after dwelling at 100 °C for 2 h with an argon flow of 100 mL min^{-1}. A Fourier transform infrared spectroscopy (FTIR) spectrophotometer (PerkimElmer Frontier) was used to record the infrared spectra using KBr pellets. The surface functional groups were analysed by X-ray photoelectron spectrometer (Thermo Fisher Scientific ThetaProbe XPS) with a monochromatic Al Kα (1486.68 eV) X-ray radiation (15 kV / 6.7 mA). C 1s line of the adventitious carbon at 285.0 eV was used as reference. The d-spacing was detected by X-ray diffraction (XRD) using Rigaku Smartlab X-ray Diffractometer. Raman spectroscopy was performed on a Renishaw Raman Microscopy with 2.33 eV (532 nm) excitation laser.

Electrochemical measurement:

Commercial MWCNT, GNP, and synthesized MWCNT@GONR were used as active material. Each active material was mixed with carbon black as conducting agent (super P, Sigma-Aldrich) and sodium carboxymethyl cellulose (CMC) (Sigma-Aldrich) as binder in a solution of DI water : methanol (1 : 1 weight %) with a weight ratio of 80 : 10 : 10 to prepare the active layer of the electrodes. The slurry was stirred overnight and coated onto a copper foil using a doctor blade with a height of 75 mm; the coating was dried in air at 80 °C to remove the solvent. The dried coating was punched into pieces with a diameter of 10 mm and roll-pressed under 5 Pa, followed by drying in an oven at 110 °C under vacuum overnight. These coated foils were assembled in 2016 coin cells with circular metallic sodium metal (diameter 16 mm) as the counter electrode, and glass fiber (Whatman) with a diameter of 19 mm as separator. 1M

$NaClO_4$ in a mixture of ethylene carbonate (EC) and propylene carbonate (PC) (1:1 weight %) was used as electrolyte. A Bio-Logic SP300 potentiostat was employed to measure cyclic voltammetry, and a Neware battery tester was utilized for galvanostatic charge / discharge tests in the range of 0.01 V – 3 V vs. Na/Na^+.

Full cell investigations

A full cell fabricated with MWCNT@GONR anode and P2-Na_xMnO_2 cathode was utilized to investigate the potential of MWCNT@GONR in a Na metal-free battery. The P2-$Na_{0.7}MnO_2$ cathode material was synthesized according to our previous publication.[54] NH_4HCO_3 was dissolved in deionized water following by the addition of a small amount of ethanol and a solution of $MnSO_4$ in deionized water drop wisely. This solution was stirred at room temperature to form spherical $MnCO_3$. After filtration, the precipitate was washed with water and ethanol for several times, and annealed in air for 5 h at 400 °C, resulting in the formation of spherical MnO_2. This powder was dispersed in a solution of NaOH in deionized water and ethanol. After evaporating the solvents, the residue was annealed in air for 3 h at 320 °C and then 4 h at 800 °C to obtain spherical P2-Na_xMnO_2. The cathode active material were prepared by mixing P2-Na_xMnO_2 with acetylene black as conducting agent (Alfa Aesar) and polyvinylidene fluoride (PVDF, Arkema, Kynar HSV 900) binder in the weight ratio 60:20:20 with N-methyl-2-pyrrolidone (NMP) to form a homogeneous slurry. This mixture was coated on an aluminum foil using a doctor blade; the coating was dried in air at 80 °C to remove the NMP. The coating was punched into pieces with a diameter of 16 mm and roll-pressed, followed by drying in an oven at 110 °C under vacuum overnight. Both MWCNT@GONR anode and P2-Na_xMnO_2 cathode were tested in half-cells with a current density of 20 mA g^{-1} in order to calculate the mass ratio. The MWCNT@GONR half-cell was cycled for 5 times and kept at 2.2 V vs. Na/Na^+, while the P2-$Na_{0.7}MnO_2$ half-cell was cycled for 2 time and kept at 2.2 V vs. Na/Na^+. Those electrodes were then fabricated as a full cell with a matched

mass ratio. The full cell was charged and discharged between a voltage of 0 ~ 4 V at a current density of 20 mA g^{-1} based on the mass of anode active material.

Supporting Information

Supporting Information is available from the Wiley Online Library or from the author.

Acknowledgements

The authors would like to thank Ms. Jing Wang for her help with Raman measurements. This research project is funded by the National Research Foundation Singapore under its Campus for Research Excellence and Technological Enterprise (CREATE) programme (Singapore), Newcastle University (United Kingdom), and Chang Gung University (Taiwan).

Received: ((will be filled in by the editorial staff))
Revised: ((will be filled in by the editorial staff))
Published online: ((will be filled in by the editorial staff))

References

[1] H. Wang, S. Hamanaka, T. Yokoyama, H. Yoshikawa and K. Awaga, *Chemistry-an Asian Journal*, **2011**, 6, 1074-1079.
[2] Y. Wen, K. He, Y. Zhu, F. Han, Y. Xu, I. Matsuda, Y. Ishii, J. Cumings and C. Wang, *Nat Commun*, **2014**, 5.
[3] Y. X. Wang, S. L. Chou, H. K. Liu and S. X. Dou, *Carbon*, **2013**, 57, 202-208.
[4] J. C. Pramudita, D. Pontiroli, G. Magnani, M. Gaboardi, M. Ricco, C. Milanese, H. E. A. Brand and N. Sharma, *Chemelectrochem*, **2015**, 2, 600-610.
[5] N. Yabuuchi, K. Kubota, M. Dahbi and S. Komaba, *Chemical Reviews*, **2014**, 114, 11636-11682.
[6] S. Hartung, N. Bucher, H.-Y. Chen, R. Al-Oweini, S. Sreejith, P. Borah, Z. Yanli, U. Kortz, U. Stimming, H. E. Hoster and M. Srinivasan, *Journal of Power Sources*, **2015**, 288, 270-277.
[7] L. P. Wang, L. H. Yu, X. Wang, M. Srinivasan and Z. C. J. Xu, *Journal of Materials Chemistry A*, **2015**, 3, 9353-9378.
[8] A. Ponrouch, A. R. Goñi and M. R. Palacín, *Electrochemistry Communications*, **2013**, 27, 85-88.
[9] Z. H. Wang, L. Qie, L. X. Yuan, W. X. Zhang, X. L. Hu and Y. H. Huang, *Carbon*, **2013**, 55, 328-334.

[10] Y. Xu, E. Memarzadeh Lotfabad, H. Wang, B. Farbod, Z. Xu, A. Kohandehghan and D. Mitlin, *Chemical Communications*, **2013**, 49, 8973-8975.
[11] Y. Sun, L. Zhao, H. Pan, X. Lu, L. Gu, Y.-S. Hu, H. Li, M. Armand, Y. Ikuhara, L. Chen and X. Huang, *Nat Commun*, **2013**, 4, 1870.
[12] P. Senguttuvan, G. Rousse, V. Seznec, J.-M. Tarascon and M. R. Palacín, *Chemistry of Materials*, **2011**, 23, 4109-4111.
[13] Y. Wang, X. Yu, S. Xu, J. Bai, R. Xiao, Y.-S. Hu, H. Li, X.-Q. Yang, L. Chen and X. Huang, *Nat Commun*, **2013**, 4.
[14] R. Alcántara, M. Jaraba, P. Lavela and J. L. Tirado, *Chemistry of Materials*, **2002**, 14, 2847-2848.
[15] S. Hariharan, K. Saravanan, V. Ramar and P. Balaya, *Physical Chemistry Chemical Physics*, **2013**, 15, 2945-2953.
[16] S. Hariharan, K. Saravanan and P. Balaya, *Electrochemistry Communications*, **2013**, 31, 5-9.
[17] S. Yuan, X.-l. Huang, D.-l. Ma, H.-g. Wang, F.-z. Meng and X.-b. Zhang, *Advanced Materials*, **2014**, 26, 2273-2279.
[18] H.-S. Ryu, J.-S. Kim, J. Park, J.-Y. Park, G.-B. Cho, X. Liu, I.-S. Ahn, K.-W. Kim, J.-H. Ahn, J.-P. Ahn, S. W. Martin, G. Wang and H.-J. Ahn, *Journal of Power Sources*, **2013**, 244, 764-770.
[19] Z. Hu, L. Wang, K. Zhang, J. Wang, F. Cheng, Z. Tao and J. Chen, *Angewandte Chemie*, **2014**, 126, 13008-13012.
[20] T. Zhou, W. K. Pang, C. Zhang, J. Yang, Z. Chen, H. K. Liu and Z. Guo, *ACS Nano*, **2014**, 8, 8323-8333.
[21] Q. Su, G. Du, J. Zhang, Y. Zhong, B. Xu, Y. Yang, S. Neupane and W. Li, *ACS Nano*, **2014**, 8, 3620-3627.
[22] Z. Shadike, Y.-N. Zhou, F. Ding, L. Sang, K.-W. Nam, X.-Q. Yang and Z.-W. Fu, *Journal of Power Sources*, **2014**, 260, 72-76.
[23] Y.-X. Wang, S.-L. Chou, H.-K. Liu and S.-X. Dou, *Carbon*, **2013**, 57, 202-208.
[24] J. Qian, X. Wu, Y. Cao, X. Ai and H. Yang, *Angewandte Chemie*, **2013**, 125, 4731-4734.
[25] W.-J. Li, S.-L. Chou, J.-Z. Wang, H.-K. Liu and S.-X. Dou, *Nano Letters*, **2013**, 13, 5480-5484.
[26] W. J. Li, S. L. Chou, J. Z. Wang, J. H. Kim, H. K. Liu and S. X. Dou, *Advanced Materials*, **2014**, 26, 4037-4042.
[27] Y. Kim, Y. Kim, A. Choi, S. Woo, D. Mok, N.-S. Choi, Y. S. Jung, J. H. Ryu, S. M. Oh and K. T. Lee, *Advanced Materials*, **2014**, 26, 4139-4144.
[28] V. L. Chevrier and G. Ceder, *Journal of The Electrochemical Society*, **2011**, 158, A1011-A1014.
[29] A. Darwiche, C. Marino, M. T. Sougrati, B. Fraisse, L. Stievano and L. Monconduit, *Journal of the American Chemical Society*, **2012**, 134, 20805-20811.
[30] D. Bresser, F. Mueller, D. Buchholz, E. Paillard and S. Passerini, *Electrochimica Acta*, **2014**, 128, 163-171.
[31] S.-M. Oh, S.-T. Myung, M.-W. Jang, B. Scrosati, J. Hassoun and Y.-K. Sun, *Physical Chemistry Chemical Physics*, **2013**, 15, 3827-3833.
[32] J.-C. Kim and D.-W. Kim, *Electrochemistry Communications*, **2014**, 46, 124-127.
[33] J. R. Gonzalez, F. Nacimiento, R. Alcantara, G. F. Ortiz and J. L. Tirado, *CrystEngComm*, **2013**, 15, 9196-9202.
[34] J. S. Thorne, R. A. Dunlap and M. N. Obrovac, *Electrochimica Acta*, **2013**, 112, 133-137.
[35] T. Yamamoto, T. Nohira, R. Hagiwara, A. Fukunaga, S. Sakai, K. Nitta and S. Inazawa, *Electrochimica Acta*, **2014**, 135, 60-67.

[36] M. He, K. Kravchyk, M. Walter and M. V. Kovalenko, *Nano Letters*, **2014**, 14, 1255-1262.
[37] P. R. Abel, Y.-M. Lin, T. de Souza, C.-Y. Chou, A. Gupta, J. B. Goodenough, G. S. Hwang, A. Heller and C. B. Mullins, *The Journal of Physical Chemistry C*, **2013**, 117, 18885-18890.
[38] C. Nithya and S. Gopukumar, *Journal of Materials Chemistry A*, **2014**, 2, 10516-10525.
[39] C. Nithya and S. Gopukumar, *Chemsuschem*, **2013**, 6, 898-904.
[40] V. Gupta and T. Saleh, *Syntheses of Carbon Nanotube-Metal Oxides Composites; Adsorption and Photo-degradation*, 2011.
[41] V. J. Cruz-Delgado, B. L. Espana-Sanchez, C. A. Avila-Orta and F. J. Medellin-Rodriguez, *Polymer Journal*, **2012**, 44, 952-958.
[42] L. I. Nasibulina, I. V. Anoshkin, A. G. Nasibulin, A. Cwirzen, V. Penttala and E. I. Kauppinen, *Journal of Nanomaterials*, **2012**.
[43] S. Hussain, P. Jha, A. Chouksey, R. Raman, S. S. Islam, T. Islam and P. K. Choudhary, *Journal of Modern Physics*, **2011**, Vol.02No.06, 6.
[44] L. Y. Lin, M. H. Yeh, J. T. Tsai, Y. H. Huang, C. L. Sun and K. C. Ho, *Journal of Materials Chemistry A*, **2013**, 1, 11237-11245.
[45] L. David and G. Singh, *The Journal of Physical Chemistry C*, **2014**, 118, 28401-28408.
[46] J. Friedl, C. M. Bauer, A. Rinaldi and U. Stimming, *Carbon*, **2013**, 63, 228-239.
[47] S. H. Huh, in *Physics and Applications of Graphene - Experiments*, ed. S. Mikhailov, InTech, Rijeka, Croatia, 2011, ch. 5, pp. 73-90.
[48] C. Bommier, W. Luo, W.-Y. Gao, A. Greaney, S. Ma and X. Ji, *Carbon*, **2014**, 76, 165-174.
[49] A. Choi, Y. K. Kim, T. K. Kim, M. S. Kwon, K. T. Lee and H. R. Moon, *Journal of Materials Chemistry A*, **2014**, 2, 14986-14993.
[50] J. Jin, Z.-q. Shi and C.-y. Wang, *Electrochimica Acta*, **2014**, 141, 302-310.
[51] H. W. Nesbitt, G. M. Bancroft, G. S. Henderson, R. Ho, K. N. Dalby, Y. Huang and Z. Yan, *Journal of Non-Crystalline Solids*, **2011**, 357, 170-180.
[52] M. A. Muñoz-Márquez, M. Zarrabeitia, E. Castillo-Martínez, A. Eguía-Barrio, T. Rojo and M. Casas-Cabanas, *ACS Applied Materials & Interfaces*, **2015**, 7, 7801-7808.
[53] B. W. Xiao, X. F. Li, X. Li, B. Q. Wang, C. Langford, R. Y. Li and X. L. Sun, *Journal of Physical Chemistry C*, **2014**, 118, 881-890.
[54] N. Bucher, S. Hartung, A. Nagasubramanian, Y. L. Cheah, H. E. Hoster and S. Madhavi, *Acs Applied Materials & Interfaces*, **2014**, 6, 8059-8065.
[55] H.-Y. Chen , G. Wee , R. Al-Oweini, J. Friedl , K. S. Tan, Y. Wang, C. L. Wong , U. Kortz, U. Stimming and M. Srinivasan, *ChemPhysChem*, **2014**, 15, 2162-2169.
[56] X. H. Ma, H. L. Chen and G. Ceder, *Journal of the Electrochemical Society*, **2011**, 158, A1307-A1312.
[57] D. Y. W. Yu, P. V. Prikhodchenko, C. W. Mason, S. K. Batabyal, J. Gun, S. Sladkevich, A. G. Medvedev and O. Lev, *Nat Commun*, **2013**, 4.
[58] C. L. Sun, C. T. Chang, H. H. Lee, J. G. Zhou, J. Wang, T. K. Sham and W. F. Pong, *Acs Nano*, **2011**, 5, 7788-7795.

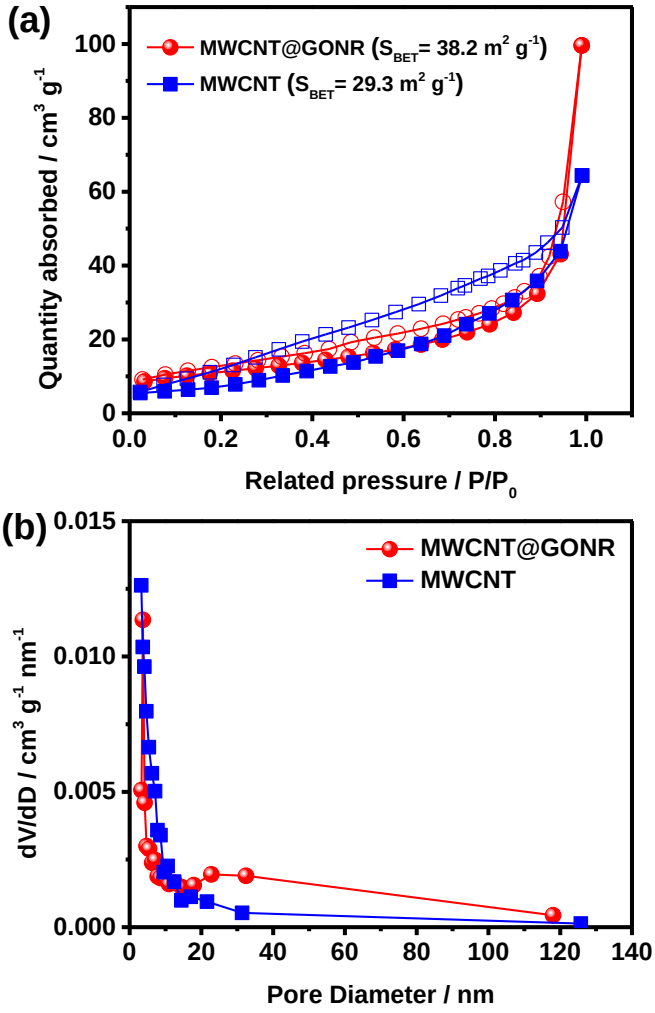

Figure 1. (a) BET graph and (b) the corresponding BJH pore size distribution curve of MWCNT and MWCNT@GONR determined by N_2 adsorption-desorption isotherms, where V is the total volume and D is the pore diameter.

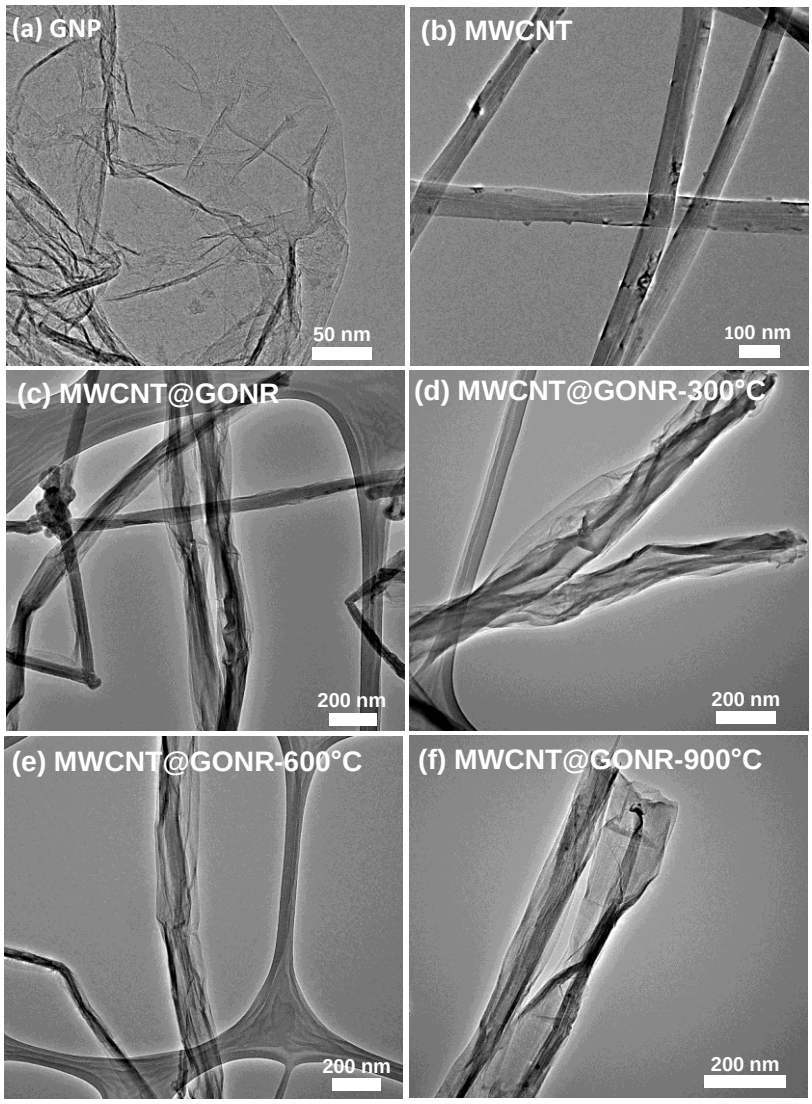

Figure 2. TEM images of (a) GNP, (b) MWCNT, (c) MWCNT@GONR, (d) MWCNT@GONR-300°C, (e) MWCNT@GONR-600°C, and (f) MWCNT@GONR-900°C

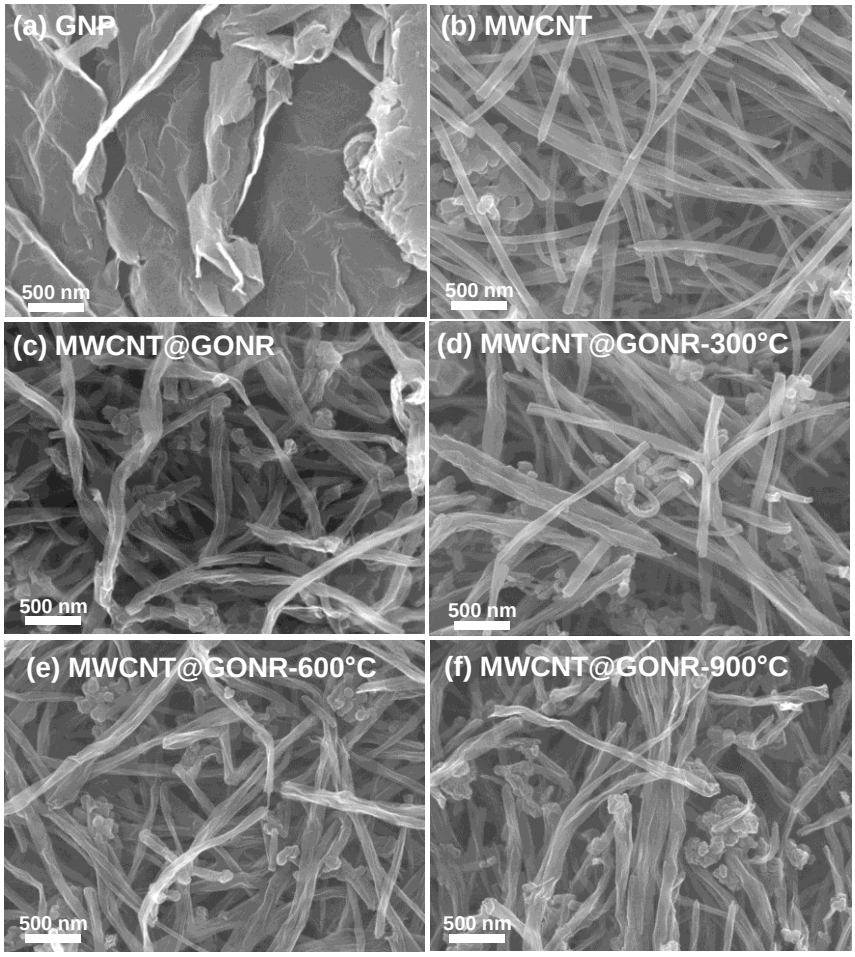

Figure 3. FESEM images of (a) GNP, (b) MWCNT, (c) MWCNT@GONR, (d) MWCNT@GONR-300°C, (e) MWCNT@GONR-600°C, and (f) MWCNT@GONR-900°C

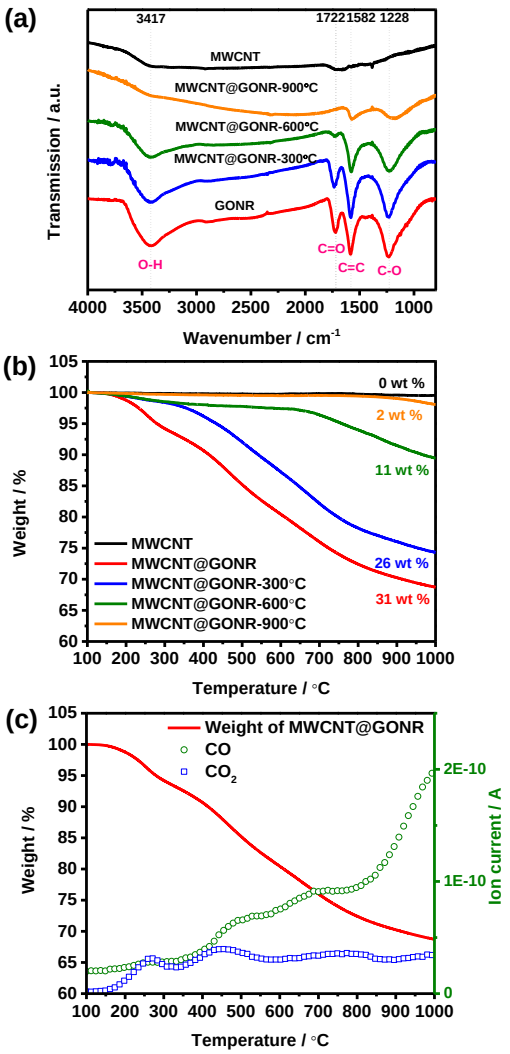

Figure 4. (a) FTIR spectrum and (b) TGA spectrum of MWCNT, MWCNT@GONR, MWCNT@GONR-300°C, MWCNT@GONR-600°C, and MWCNT@GONR-900°C; (c) MS spectrum of MWCNT@GONR

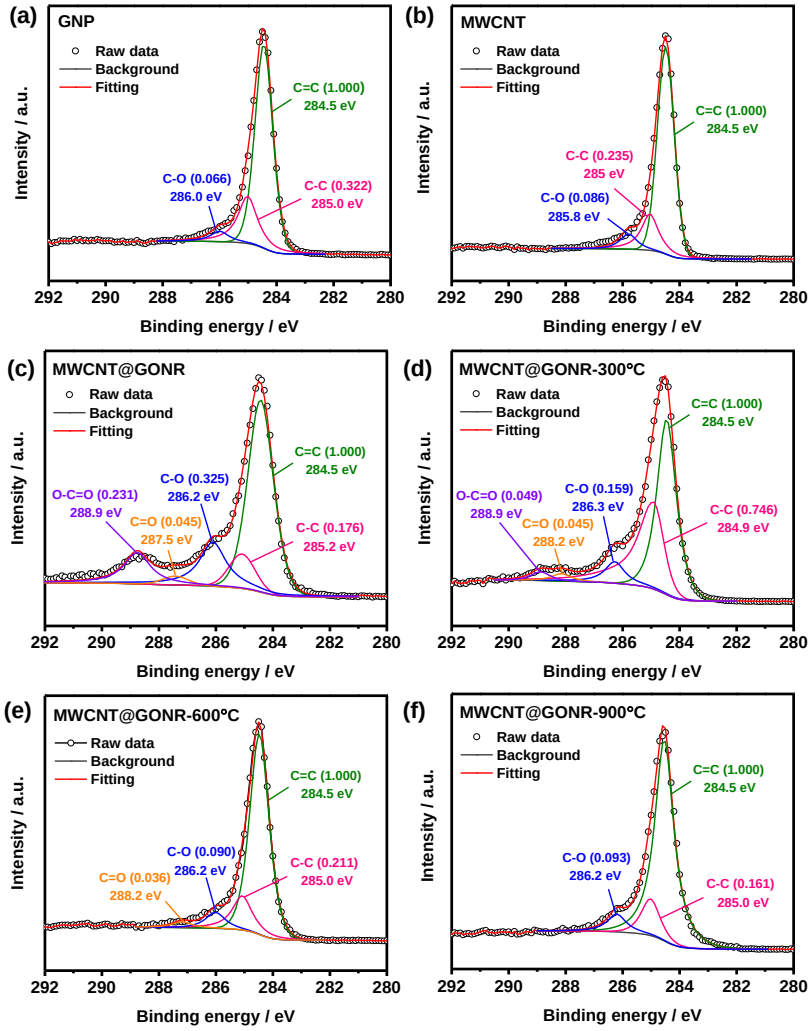

Figure 5. XPS spectrum of (a) GNP, (b) MWCNT, (c) MWCNT@GONR, (d) MWCNT@GONR-300°C, (e) MWCNT@GONR-600°C, and (f) MWCNT@GONR-900°C

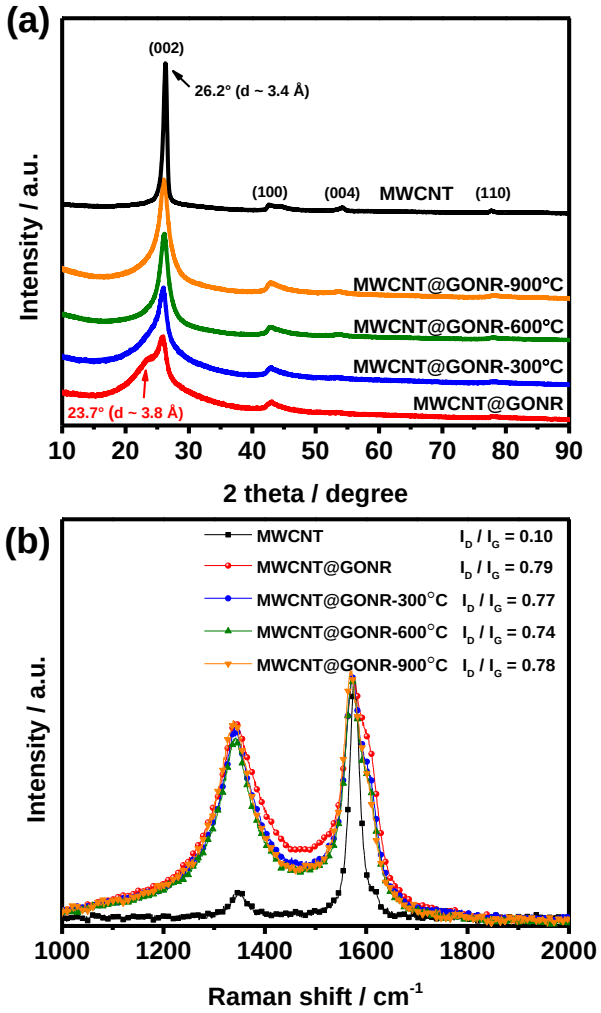

Figure 6. (a) XRD spectrum and (b) Raman spectrum of MWCNT, MWCNT@GONR, MWCNT@GONR-300°C, MWCNT@GONR-600°C, and MWCNT@GONR-900°C

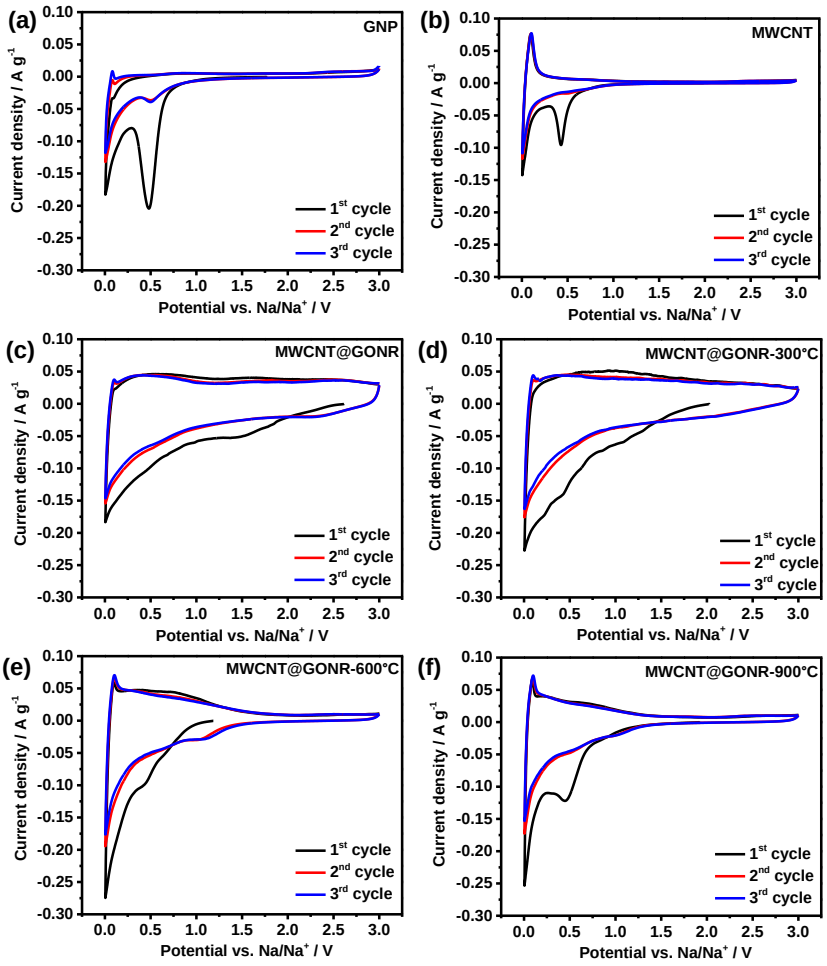

Figure 7. Cyclic voltammograms measured at 0.1 mV s^{-1} of (a) GNP, (b) MWCNT, (c) MWCNT@GONR, (d) MWCNT@GONR-300°C, (e) MWCNT@GONR-600°C, and (f) MWCNT@GONR-900°C in the potential range of 0.005 ~ 3 V vs. Na/Na^+ with 1M $NaClO_4$ in EC:PC (1:1 weight %) as electrolyte.

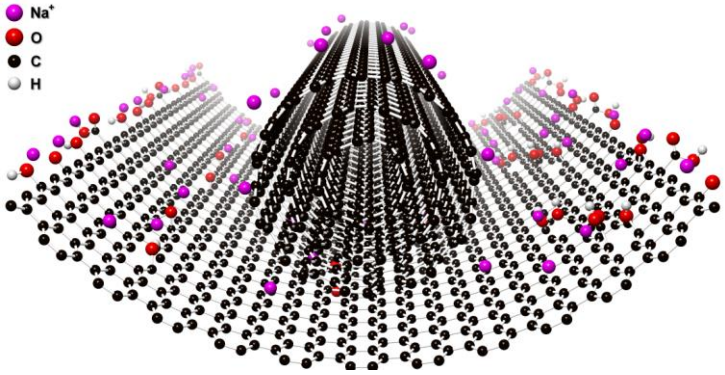

Scheme 1. Schematic diagrams of insertion/adsorption of sodium ions into/onto MWCNT@GONR

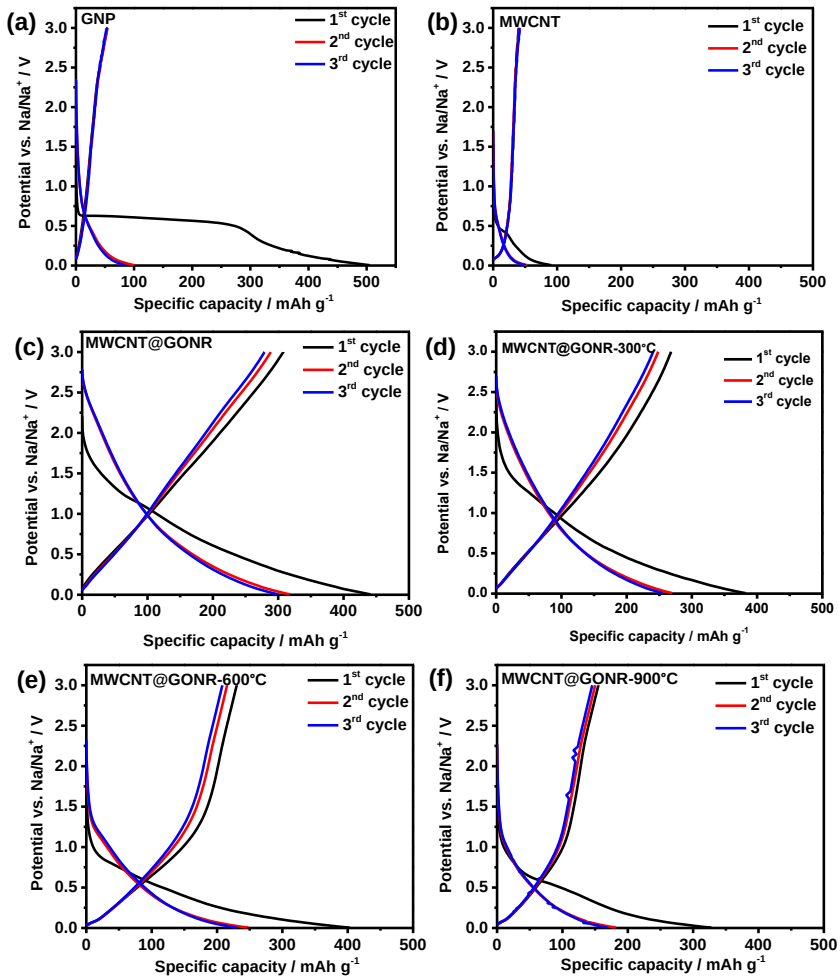

Figure 8. The galvanostatic charge-discharge curves at current density of 50 mA g^{-1} of (a) GNP, (b) MWCNT, (c) MWCNT@GONR, (d) MWCNT@GONR-300°C, (e) MWCNT@GONR-600°C, and (f) MWCNT@GONR-900°C in the potential range of 0.005 ~ 3 V vs. Na/Na^+ with 1M $NaClO_4$ in EC:PC (1:1 weight %) as electrolyte.

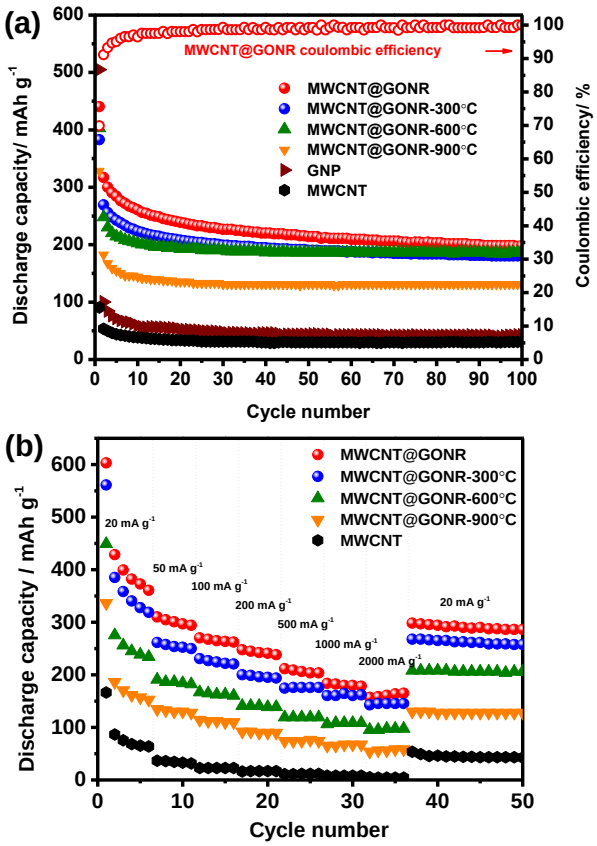

Figure 9. (a) The cycling performance of GNP, MWCNT, MWCNT@GONR, MWCNT@GONR-300°C, MWCNT@GONR-600°C, and MWCNT@GONR-900°C measured at current density of 50 mA g^{-1} with 1M $NaClO_4$ in EC:PC (1:1 weight %) as electrolyte. (b) The rate capability and stability of GNP, MWCNT, MWCNT@GONR, MWCNT@GONR-300°C, MWCNT@GONR-600°C, and MWCNT@GONR-900°C measured at current density of 20, 50, 100, 200, 500, 1000, 2000, and 20 mA g^{-1} with 1M $NaClO_4$ in EC:PC (1:1 weight %) as electrolyte.

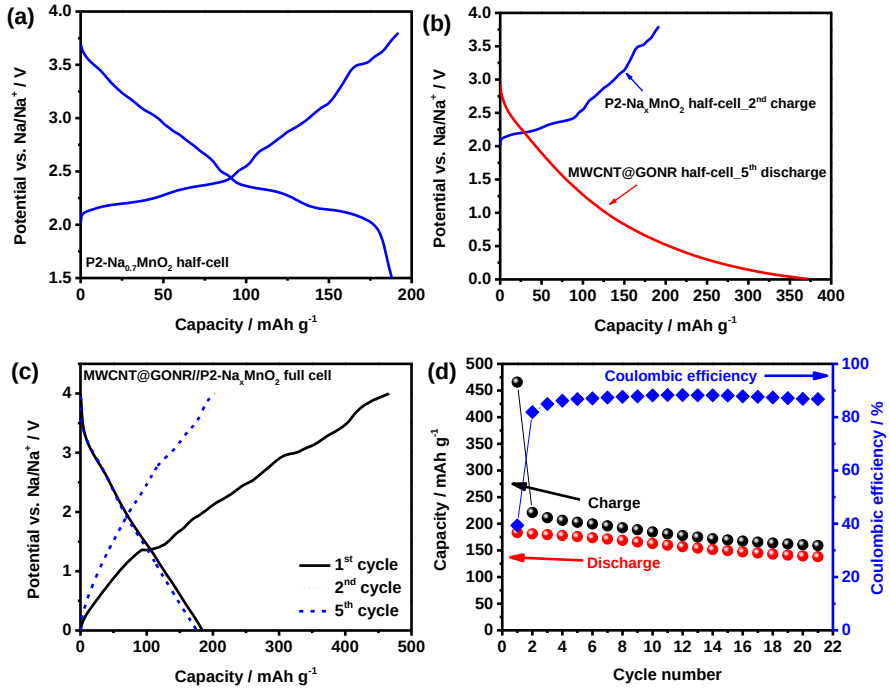

Figure 10. Proof of concept for a MWCNT@GONR–based full cell set-up using MWCNT@GONR as anode and P2-Na_xMnO_2 as cathode with 1M $NaClO_4$ in EC:PC (1:1 weight %) as electrolyte. (a) The galvanostatic charge-discharge curves of the P2-$Na_{0.7}MnO_2$ half-cell at current density of 20 mA g^{-1} in a potential range: 1.5 – 3.8 V vs. Na/Na^+. (b) The galvanostatic charge-discharge curves of MWCNT@GONR half-cell at 5th discharging and P2-Na_xMnO_2 half-cell at 2nd charging at current density of 20 mA g^{-1}. (c) The full cell galvanostatic charge-discharge curves and (d) the charge / discharge capacities with respect to the mass of MWCNT@GONR as well as the corresponding coulomb efficiencies at current density of 20 mA g^{-1} in a potential range: 0 – 4 V.